Bioactive Glass/Polycaprolactone Hybrid with a Dual Cortical/Trabecular Structure for Bone Regeneration

Henri Granel, Cédric Bossard, Anne-Margaux Collignon, Fabien Wauquier, Julie Lesieur, Gael Rochefort, Edouard Jallot, Jonathan Lao, Yohann Wittrant

Article type: Full Paper

Bioactive Glass / Polycaprolactone Hybrid with Dual Cortical / Trabecular Structure for Bone Regeneration

Granel Henri, Bossard Cédric, Collignon Anne-Margaux, Wauquier Fabien, Lesieur Julie, Rochefort Gael Y, Jallot Edouard, Lao Jonathan, Wittrant Yohann**

Dr. Granel. Author 1, Dr. Wauquier. Author 4, Dr. Wittrant. Author 9.
Human Nutrition Unit - UMR1019 - INRA Research Center, 63122, France
E-mail: henri.granel@inra.fr
Dr. Bossard. Author 2, Prof. Jallot. Author 7, Dr. Lao. Author 8.
Laboratoire de Physique de Clermont-Ferrand, 4 Avenue Blaise Pascal - BP 80026 – 63177, France
Prof. Rochefort. Author 6, Dr Collignon. Author 3, Lesieur. Author 5
Faculté de Chirurgie Dentaire - Paris Descartes - EA2496 - Laboratoires Pathologies, Imagerie et Biothérapies orofaciales - 1 rue Maurice Arnoux – 92120, France

Abstract

Organic-inorganic hybrid biomaterials stand as a promise for combining bone bonding and bone mineral-forming ability, stimulation of osteogenic cells and adequate mechanical properties. Bioactive glass (BG) – polycaprolactone (PCL) hybrids are of special interest as they gather the ability of BG to enhance osteoblast-mediated bone formation with the slow degradation rate and the toughness of PCL. In this study, BG-PCL hybrids were synthesized in the form of scaffold owing a dual cortical/trabecular structure mimicking the bone architecture. Their biological potential was evaluated both *in vitro* using rat primary osteoblasts (RPO) and *in vivo* in a mice model of critical-size calvarial defects. BG-PCL were compared to Lubboc^{TM} (BTB), a commercial purified bovine xenograft widely used in orthopedics and periodontal procedures and known for its efficiency. BG-PCL hybrids were found to facilitate RPO adhesion at their surface and to enhance RPO differentiation when compared to BTB. *In vivo* micro-CT study demonstrates a higher bone ingrowth with BG-PCL scaffolds and a complete chemical conversion of remaining BG-PCL after 3 months

implantation, while histological data show the vascularization of BG-PCL scaffolds and confirm the well-advanced bone regeneration with ongoing remodeling. Finally, we evidence the complete chemical conversion of remaining BG-PCL into a bone-like mineral.

Keywords: Bioactive glass; Polycaprolactone; Hybrid; Scaffold; Synthetic bone substitute; Bone regeneration

1. Introduction

The search for a synthetic bone substitute able to perform as well as autologous bone grafts is a constant concern in bone tissue engineering. In this light, bioactive glasses (BG) have attracted ever growing attention due to their biological properties such as bone bonding,[1] osteogenic stimulation,[2,3] pro-angiogenic and antibacterial properties.[4–6] However, the clinical use of BG has been limited so far by several factors including the poor variety of shapes for the implanted material and their inherent brittleness (both being associated). BG can be synthesized into macroporous structures required for guiding the bone regeneration in case of major trauma and large bone defects, but the resulting BG scaffolds suffer from brittleness and may collapse under physiological cyclic loading due to their poor resistance to crack propagation.[7] In order to improve the toughness and resilience of the material, BG particles can be dispersed in a bioresorbable polymer matrix to produce osteogenic BG-polymer composites. However, it is very difficult to control the exposure of BG particles to the external environment at the surface of the polymer and thereby to control the bioactive and osteogenic properties of the composite [8]. To address those limitations, organic-inorganic hybrids associating BG and polymers have been developed. In these hybrids, chains of BG nanoparticles (2-4 nm) produced by sol-gel chemistry may entangle with polymer chains {ref: revue Jones}. The organic and inorganic networks can be interpenetrated at the molecular level, which results in uniform properties above the nanoscale [9]. Other key advantages of hybrids are their tailorable degradation rate and mechanical properties {ref: Zhao et al. *A highly bioactive and biodegradable poly(glycerol sebacate)–silica glass hybrid elastomer with tailored mechanical properties for bone tissue regeneration*, Kascholke et al. *Biodegradable and adjustable sol-gel glass based hybrid scaffolds from multi-armed oligomeric building blocks*, Mondal et al. *Porous and biodegradable polycaprolactone-borophosphosilicate hybrid scaffolds for osteoblast infiltration and stem cell differentiation*}

and the possibility to incorporate organic and inorganic species that present a therapeutic effect, *e.g.* osteogenic, angiogenic or antibacterial {ref: Granel et al.}. So far, the development of bioactive hybrids has been hindered by the complexity of their synthesis, which relies on the sol-gel process. Indeed, the use of a polymer at the early stage of the sol-gel process forbids the use of thermal treatments, which are commonly employed for the incorporation of calcium ions into the BG silicate network.[10] Calcium plays a major role in the bioactivity of BG and it is involved in osteoblasts proliferation and differentiation.[11] The difficulties arising from the synthesis of calcium-containing hybrids might explain why in the literature, studies mainly focus on pure silica-based hybrids that possess a limited apatite-forming ability {ref: Hendrikx et al. *Indirect rapid prototyping of sol-gel hybrid glass scaffolds for bone regeneration – Effects of organic crosslinker valence, content and molecular weight on mechanical properties*, Sang et al. *Hybrids of silica/poly(caprolactone coglycidoxypropyl trimethoxysilane) as biomaterials*, Tallia et al. *Bouncing and 3D printable hybrids with self-healing properties*}, or focus on other potentially bioactive systems such as borophosphosilicate glass-polymer hybrids {ref: Mondal et al. *Bioactive borophosphosilicate-polycaprolactone hybrid biomaterials via a non-aqueous sol gel process*, Mondal et al. *Mechanically-competent and cytocompatible polycaprolactone-borophosphosilicate hybrid biomaterials*}, or involve the use of calcium salt precursors {ref: Rhee et al. *Bone-like apatite-forming ability and mechanical properties of PCL/silica hybrid as a function of PCL content*, Allo et al. *Hydroxyapatite formation on sol–gel derived polycaprolactone/bioactive glass hybrid biomaterials*, Ding et al. *Electrospun polyhydroxybutyrate/poly(ε-caprolactone)/58S sol–gel bioactive glass hybrid scaffolds with highly improved osteogenic potential for bone tissue engineering*} that are known to induce heterogeneous calcium distribution in the material {ref: Lin et al. *Nanostructure evolution and calcium distribution in sol-gel derived bioactive glass*, Yu et al. *Effect of calcium source on structure and properties of sol-gel*

derived bioactive glasses}. Some BG-polymer hybrids with well-incorporated calcium have been successfully synthetized but under the form of dense[12,13] or fiber[14] materials. In a work from Lao *et al.*, BG (SiO_2-CaO)-gelatin hybrid scaffolds were fabricated at room temperature with a homogeneous incorporation of calcium thanks to the use of calcium ethoxide precursor.[15] With a similar process, Bossard *et al.* recently produced BG (SiO_2-CaO)-polycaprolactone (PCL) hybrid scaffolds [16] that proved to degrade at a more adequate rate with regard to bone regeneration. To our knowledge, these BG-polymer hybrids are the first to exhibit both a well-interconnected macroporous structure and homogeneous calcium incorporation in the silicate network. Interestingly, calcium incorporation resulted in an extended apatite-forming ability with the entire hybrid material being massively changed into bone-like minerals (while apatite formation is traditionally limited to a thin surface layer – a few μm thick – with BG[17]).

Versatility is a key advantage of the BG hybrids synthesis process we have developed. It allows the development of complex structures mimicking the bone architecture. We have recently succeeded in obtaining dual structures associating highly porous trabecular-like regions to dense cortical-like regions. Such a dual structure may be of particular interest in maxillofacial surgery applications where bone regeneration needs to be prevented from connective and epithelial soft tissues. Currently, resorbable or non-resorbable synthetic membranes are used to play the physical role of barrier and/or to limit the resorption of the bone graft. Non-resorbable membranes like PTFE need to be fixed with screws and therefore require a second intervention to remove them. On the other hand, resorbable membranes (for instance collagen-based membranes) reduce postoperative complications, but still require to be supported by a bone-filling material.[18] In contrast, a single implant with a dual porous / dense structure has the major advantage of displaying full physical and chemical continuity between the porous part, intended to receive bone ingrowth, and the dense part, acting as a

barrier. Moreover, in orthopedics the thickness required for the dense part of the implant can be substantial, up to several millimeters. Currently, only autografts or allografts can match these criteria since they are the only sources of mixed trabecular/cortical bones with sufficiently thick cortical parts. Hence, the development of synthetic scaffolds owing a mixed architecture would open interesting perspectives.

As a consequence, we investigated in this work the biological relevance of BG-PCL hybrid scaffolds through a thorough *in vitro* study and of hybrid scaffolds owing a dual cortical/trabecular structure through an *in vivo* study in a critical-size mouse calvarial defect model. The biological properties of BG-PCL hybrids are compared to a commercial standard known for its biological performance, namely a purified bovine trabecular bone (BTB) consisting of bone mineral with residual collagen used in orthopedics and periodontal surgery procedures. The physicochemical properties of BG-PCL hybrid scaffolds were assessed in a previous study {ref: Bossard et al.}. The scaffolds possess a total porosity of 69 ± 1% (including a close porosity of barely 0.1%) with pores ranging from 300 to 500 µm and interconnections ranging from 150 to 200 µm, they present a non-fragile behavior and are highly flexible with an elastic modulus of 0.49 ± 0.03 MPa and yield strength of 0.036 ± 0.003 MPa, and they degrade slowly with a 13.2% weight loss after 8 weeks of soaking in Simulated Body Fluid.

2. Material and methods

2.1. Synthesis of BG-PCL hybrid scaffolds

Hybrid scaffolds composed of 30 wt.% BG – 70 wt.% PCL were fabricated at room temperature using the sol-gel process previously developed by Bossard *et al.*[16] Briefly, tetraethyl orthosilicate (TEOS) (99% purity, Aldrich) is hydrolyzed for 30 min in ethanol

(absolute, Aldrich) by adding an HCl solution (2 M, Aldrich) (molar ratio ethanol : H_2O : TEOS : HCl = 3.7 : 2 : 1 : 0.07). Calcium ethoxide (95% purity, Gelest) diluted in the same volume of ethanol is then added to the solution to reach a BG composition of 75 wt.% SiO_2 – 25 wt.% CaO and the obtained sol is left for condensation. PCL (M_n = 80000 $g.mol^{-1}$, Aldrich) is dissolved in tetrahydrofuran (18.2 w/v %) and then mixed with the inorganic sol right before its gelation. The resultant hybrid solution is left for 1 hour for homogenization and further condensation. Afterwards, scaffolds are produced using a porogen leaching method. First, paraffin microspheres are made-up by emulsifying paraffin in hot water as described by Ma *et al.*[19] Microspheres of 400-600 µm are then selected by sieving, stacked into polyethylene molds and heated 60 min at 40°C to partially fuse them. The hybrid solution is infiltrated into the template by centrifugation (6000 rpm) and left for gelation (72h). Finally, the material is immersed in three consecutive 24 h cyclohexane baths to remove the porogen (a macroporous structure is therefore obtained) and rinsed in absolute ethanol for 24 h. The obtained scaffolds are naturally surrounded by a dense layer of hybrid material, and its thickness can be further increased by increasing the volume ratio of hybrid solution/stack of microsphere (*i.e.* the amount of supernatant hybrid solution above the stack of porogen microspheres). Here a 3 µm dense layer was generated at the bottom of the scaffolds.

2.2. *In vitro* study

2.2.1. Isolation and culture of osteoblastic cells

Rat primary osteoblastic (RPO) cells were enzymatically isolated from explant obtained from fetal Wistar rat calvaria as previously described.[20–22] Briefly, bone pieces were digested sequentially in a solution of α-MEM, penicillin/streptomycin (p/s, 1%), collagenase IA (0.1%), dispase II (0.2%) at 37°C and incubated 15 minutes 4 times at 37°C. The obtained rat calvaria cells were pooled and plated together in a 225 cm² tissue culture dishes at a density of

10,000 cells/cm^2. Cells were cultured until confluency in α-MEM medium supplemented with 10% fetal bovine serum (FBS) and 1% p/s in controlled atmosphere (5% CO_2 / 95% air, 90% hygrometry and 37°C). Then, cells were collected and frozen in 20% FBS, 7% dimethyl sulfoxide, 73% α-MEM for further use.

For cultures of RPO inside fully cortical BG-PCL scaffolds (diameter: 10 mm; height 2 mm), on pure PCL and BG-PCL disks (obtained by flattening scaffolds) and on human cortical bone slice (OST Développement), the materials were slightly glued to the bottom of the culture surfaces in 12-well-plates. Wells were then filled with 2 ml of α-MEM medium each and placed in a vacuum chamber for 72h to remove air bubbles trapped in the scaffold pores and to avoid exposing the cells to the burst of ionic dissolution products observed just after the soaking of bioactive glass scaffolds according to Radin *et al.*[23]

RPO were then added drop-wise on the material to reach 100,000 cells/material. Seeded materials were left 40 minutes at 37°C (5% CO_2 and 90% hygrometry) to allow cell adhesion. Wells were then carefully completed up to 2 mL with α-MEM supplemented with 10% FBS and 1% p/s. Cells cultured inside scaffolds were conducted under orbital agitation while no agitation was required for cells cultured on disks and human cortical bone. This 3D context of culture requires dynamic conditions. Indeed, a gradient of oxygen is observed inside scaffolds under static culture conditions that leads to a poor cell adhesion and survival at the center of the scaffolds.[24] An optimal orbital speed of 10 rpm with a 12° slot was selected according to Perez et al. who demonstrated better cell adhesion with low agitation speed. [25] The culture media were changed every two days.

2.2.2. Dissolution profile

After 72h period under vacuum, the media soaking materials was renewed (preconditioning step). Media were then collected and replaced every two days for a total period of 14 days of

culture at 37°C / 5% CO_2 and 90% hygrometry. The collected media were 0.2 µm filtered and the Ca, P and Si concentrations were determined by ICP-AES.

2.2.3. Cell viability assay

RPO were seeded on the surface of 12-well plates at a density of 10,000 cells/cm² and cultured for a total period of 7 days. To investigate dissolution product impact on cell behavior, materials were placed in cell culture inserts equipped with a membrane with a pore size of 8 µm (Falcon) and the inserts were positioned in the well plates. The cell viability was determined by an XTT based method, using the Cell Viability/Proliferation Kit II (Sigma-Aldrich) according to the supplier recommendations. The optical density (OD) was determined at 450 nm.

2.2.4. Fluorescent labelling

Cells were cultured 7 days inside BG-PCL scaffolds and BTB. Cells were labelled using a CyQUANT NF Proliferation assay kit (Invitrogen) according to the supplier recommendations and imaged by fluorescence microscopy (ZEISS Observer apotome).

2.2.5. Scanning electron microscopy (SEM)

Cells were cultured overnight either inside BG-PCL scaffolds or BTB, or at the surface of PCL or BG-PCL disks or cortical bone slices. Samples were fixed for one hour using a solution composed of glutaraldehyde (3 %) and sodium cacodylate buffer (0.2 M, pH 7.4) and then rinsed in cacodylate buffer three times for 10 min each. Afterwards, samples were dehydrated using three consecutive baths of 70, 95 and 100% ethanol for 10 min each. Finally, samples were treated in hexamethyldisilazan baths (HMDS, Delta Microscopies), dried overnight, coated using a sputter coater equipped with a gold target (Jeol JFC-1300) and observed by SEM operating at 5 keV (Jeol 6060-LV).

2.2.6. Immunoassay

Cells were cultured 7 or 14 days inside BG-PCL scaffolds and BTB. Cells were then lysed in a Nonidet P40 (NP40) lysis buffer [50 mM Tris, pH 7.4; 250 mM EDTA; 1% NP40; PMSF 1mM; protease inhibitor cocktail (Sigma Cat. # P-2714)] and subjected to western blot analysis. Equivalent amounts of total proteins were loaded and resolved on a 4-12% Bis-Tris gel (Invitrogen) and transferred to a nitrocellulose membrane (Invitrogen). Primary antibodies [Runx2, FAK, phospho-FAK (Y397), GAPDH (Cell signaling technologies)] were used, tagged with a secondary HRP-linked antibody (Cell signaling technology) and revealed by chemiluminescence using ECL reagent (Merck). Relative quantifications were performed with the ImageJ software.

2.2.7. Alkaline phosphatase activity assay

Cells were cultured inside BG-PCL scaffolds and BTB. Enzymatic alkaline phosphatase (ALP) activity was measured after 0, 7 and 14 days of culture. Afterwards, cells were washed three times with ice-cold PBS and cell lysates were prepared using NP40 lysis buffer. Cell lysates were incubated in assay buffer [40 mM *p*-nitrophenyl phosphate (Sigma Aldrich), alkaline assay buffer (Abcam)] and the production of *p*-nitrophenol was determined at 405 nm at 37°C and expressed as the mean OD per minutes. Results were normalized with respect to the GAPDH expression obtained by immunoassay.

2.3. *In vivo* study

2.3.1. Ethical and animal management

All experiments in this study were performed with a protocol approved by the Animal Care Committee of the University Paris Descartes (project agreement 17-093, APAFIS N°2018031514511875). Animals were maintained according to the guidelines for ethical

conduct developed by the European Communities Council Directive (animal breeding agreement C92-049-01). All efforts were made to minimize their pain or discomfort. C57bl6 mice were purchased from Janvier Labs (Le Genest Saint Isle, France). They were housed at 22 ± 2 °C with a 12 h dark/light cycle, and had *ad libitum* access to water and food in the animal facility of the Department of Orofacial pathologies, imagery and biotherapies of Descartes University, Montrouge, France.

2.3.2. Surgical implantation, experimental procedure and sampling

As described previously,[26] C57bl6 mice (12-weeks-old, ~30 g) were anesthetized by intraperitoneal injection of ketamine (80 mg/kg) and xylazine (10 mg/kg), both from Centravet Alfort, Maisons-Alfort, France. Scalp skin was incised, and the periosteum was discard to visualize the skull. A 3.5 mm diameter calvarial critical-sized defect was created on each side of the parietal bone using a Tissue punch (from Praxis l'Instrumentiste, France) attached to a slow-speed hand piece operating at 1,500 rpm, under irrigation with sterile saline solution. Special care was taken for the sagittal suture preservation, and minimal invasion of the dura mater. After gently removing the circular bone plug, the defects were filled with BG-PCL scaffolds or BTB. Dimensions of the cylindrical implants were 3.5 mm diameter and 1 mm height (n = 8). For each animal, the same type of material was implanted in both defects. BG-PCL scaffolds were placed in order their cortical part faced the meninges. Defects created in the skulls of 6 additional mice were left empty as negative controls ("Sham" surgery) for the critical-size defect. Wound closure was achieved by skin suturing using absorbable sutures (Vicryl Rapid 4.0, Ethicon, Johnson & Johnson). Immediate post-operative care was conducted by analgesia with buprenorphine (0.02 mg/kg b.w.). After surgery, the animals were housed individually under constant observation. No lethality was detected during the surgery nor the post-operative period. Wound healing progressed without any sign of

infection, material exposure or other complication. Body weights were examined regularly to ensure proper feeding before and after surgery. At days 0, 30, 60 and 90 post-surgery, the skull of animals were imaged by X-ray microcomputed tomography (micro-CT) as described below. All animals were euthanized at day 90 and their calvaria were excised. Samples were fixed in 70% v/v ethanol (24 h at 4 °C), dehydrated in graded ethanol solutions, and embedded at -20 °C in methyl methacrylate resin (Merck) without decalcification. Resin embedded calvarial bone samples were cut (5 mm thick) using a Jung Polycut E microtome (Leica) with hard tissue blades (Leica). After immersion in a drop of 50% v/v ethanol, sections were stretched to a fold-free state on gelatin-coated glass slides (Menzel-Gläser), or on plexiglass slides for PIXE imaging, covered with a polyethylene sheet, and tightly pressed on the glass or plexiglass slides, followed by overnight drying at room temperature. Deplastification was carried out in 2-methoxyethyl acetate (Carlo Erba) three times for 20 min. Rehydration of the sections was performed in graded ethanol solutions for subsequent procedures.

2.3.3. Micro-CT

Mice were anesthetized (isoflurane, induction at 3-4% under airflow of 0.8-1.5 L/min; 1.5-2% under 400-800 ml/min thereafter) at baseline, day 30, day 60 and day 90, and they were analysed using an X-ray micro-CT device (Quantum FX Caliper, Life Sciences, Perkin Elmer, Waltham, MA) hosted by the PIV Platform, EA2496, Montrouge, France. The X-ray source was set at 90 kV and 160 µA. Tridimensional images were acquired with an isotropic voxel size of 20 µm. An internal density phantom, calibrated in mg of hydroxyapatite, was used to scale bone density. Full 3D high-resolution raw data are obtained by rotating both the X-ray source and the flat panel detector 360° around the sample (scanning time of 3 min). Tridimensional rendering were subsequently extracted from Dicom data frames using the

open-source OsiriX imaging software (v5.7.1, distributed under LGPL license, Dr A. Rosset, Geneva, Switzerland). Quantification of the regenerated bone inside each defect was done using CTscan Analyzer software (Skyscan, release 1.13.5.1, Kontich, Belgium). A global volume of interest (VOI) was drawn by interpolating 2D region of interests on consecutive sections to isolate the initial defect area. The obtained interpolated VOI comprised only the remodeled bone defect area. A global thresholding was determined interactively for bone selection and to eliminate background noise. ‘‘New tissue” volumetric fractions were expressed relatively to the total volume of the initial defect.

2.3.4. Histological examination of samples

Deplastified hemicalvarial bone sample sections (5 mm thick) were sequentially cleared in water and stained with Von Kossa staining, Alizarine red, or processed for alkaline phosphatase (ALP) enzymohistochemistry and for tartrate-resistant acid phosphatase (TRAP) revelation. Von Kossa staining was used to visualize calcified tissues. A modified Goldner-Masson trichrome (Hematoxylin, Orange G, Ponceau Fushin, light green) was used to visualize collagen fibres, osteoid tissue and bone cells. In order to visualize osteoclast activity, TRAP was stained by using hexazotized pararosanilin (Sigma) and naphtol ASTR phosphate (Sigma, St Louis, MO); non-osteoclastic acid phosphatase was inhibited by adding 100 mM L(+)-tartric acid (Sigma, St Louis, MO) to the substrate solution. For immunohistochemistry, bone sections were rehydrated and blocked with 5% bovine serum albumin/PBS. Sections were incubated 12h at 4°C with rabbit anti-human OPN antibody (LF-175) and rat anti-EM antibody (santa cruz sc-65495) diluted at 0.5% in 5% bovine serum albumin/PBS. Sections were incubated with peroxidase-conjugated anti-IgG diluted at 1% (Dako) in 5% bovine serum albumin/PBS. Peroxidase activity was detected using a diamino-benzadine substrate kit (sigma D4293) followed by hematoxylin (vector) counterstaining. Control incubation to assess non-specific staining consisted in applying the same procedure

except that the primary antibody was substituted by nonimmune serum (control incubation were negative). Image acquisition was performed with the Leica software (LAS version 4.4) using a DMLB Leica microscope equipped with a camera (DFC425 Leica).

2.4. PIXE chemical imaging

Particle-Induced X-ray Emission (PIXE) nuclear microprobe allows studying the distribution of chemical elements down to the ppm level with a sub-micron resolution. BG-PCL scaffolds were embedded in Agar resin and cut into slices of about 150 μm thickness with a low speed diamond saw. PIXE quantitative chemical imaging was also conducted on 7.5 μm thick histological sections glued on plexiglass slides, focusing on the implant/bone interface. PIXE was carried out at the AIFIRA platform at the Centre d'Etudes Nucléaires de Bordeaux-Gradignan (CENBG, France) using a 3 MeV incident proton beam (beam diameter of 1 μm). An 80 mm^2 Si (Li) detector equipped with a 12 μm-thick beryllium window and an aluminium funny filter (a filter with a 2 mm hole drilled at its center) was used for X-ray detection and was orientated at 135° with respect to the incident beam axis. Concentrations in Ca, P and Si were determined from the recorded X-ray spectra using the Gupixwin software after calibration against the NIST 620 (soda-lime glass) standard reference material. The local mass thicknesses required for proper conversion of X-ray intensities into elemental concentrations were deduced from the Rutherford Backscattering Spectrometry (RBS) which was carried out simultaneously to PIXE using a 50 mm^2 PIPS detector (100 μm thick) orientated at 135° with respect to beam axis and placed at 19.8 mm from the sample surface. RBS spectra were treated using the SIMNRA code.

2.5. Statistics

Results in each group were expressed as the mean value ± standard deviation (SD).

For *in vitro* assay, variables were compared by analysis of variance (ANOVA) followed by two-by-two comparison performed with Tukey's HSD tests (ExcelStat Pro software – Microsoft office 2007). Statistical significance was set at $p<0.05$.

For the quantification of bone regeneration in mouse calvaria, variables were compared using one-way analysis of variance (ANOVA) followed with two-by-two comparisons performed with paired T-test of Student when they passed the Fisher F equal variance and Shapiro-Wilk normality tests. Otherwise, they were performed using Kruskal-Wallis ANOVA on the ranks followed with two-by-two comparisons performed with the U test of Mann and Whitney. Statistical significance was set at $p<0.05$.

3. Results

3.1. BG-PCL scaffolds architecture

BG-PCL scaffolds were characterized both at a macro and microscopic scale. The BG-PCL scaffolds used for implantation in mice calvarial defects show a cylindrical shape with 3.5 mm diameter and 1 mm height (**Figure. 1A**) and present a 3 μm dense layer on one side (**Figure. 1B** and **Figure. 1C**). This association of trabecular and cortical structures tends to mimic the skull bone tissue architecture. Here the cortical layer is intended to face the brain, in order to act as a protective layer for the meninges and to prevent the colonization of the scaffold by connective tissues. Cross-sectional views of the scaffolds show their well interconnected porosity of 69 ± 1%, with pore diameters and interconnections encompassing 250 – 500 μm and 150 – 200 μm respectively.[16] (**Figure. 1D**). PIXE chemical mapping demonstrates the homogeneous distribution of Si and Ca within the hybrid (**Figure. 1E**).

The BG-PCL scaffolds used for the *in vitro* tests present the same cylindrical shape with a diameter of 10 mm and a height of 2 mm and the same porosity characteristics but without the cortical part which is not necessary *in vitro*.

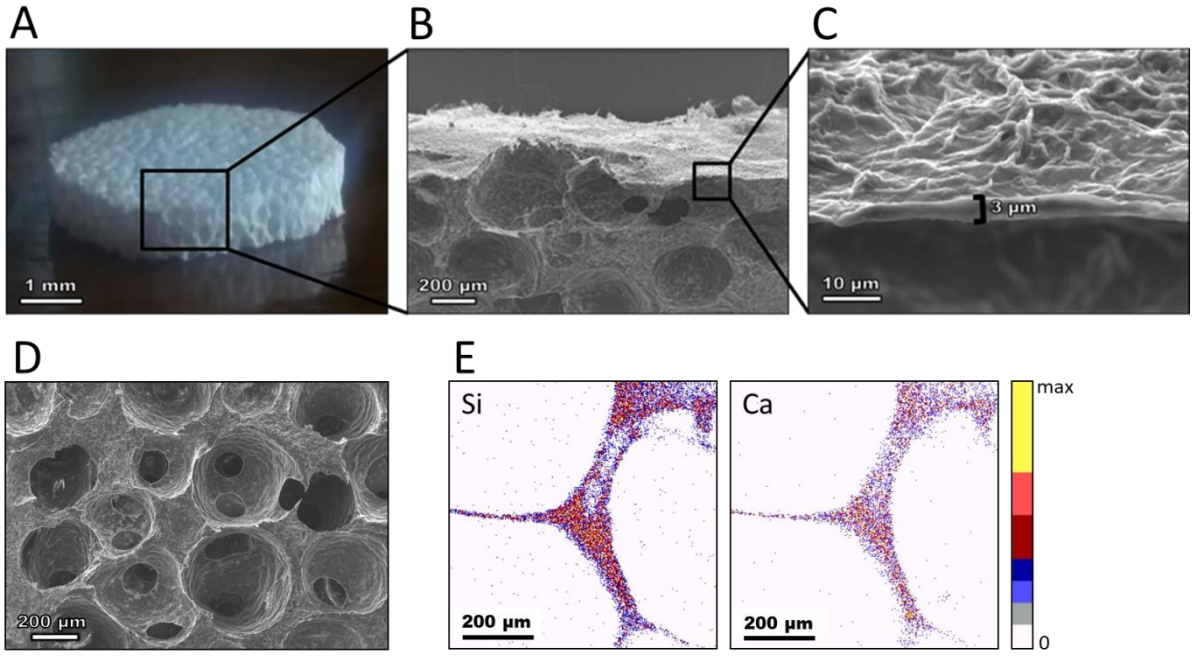

Figure 1. BG-PCL scaffolds with dual cortical/trabecular architecture. A) Global view, B) magnified SEM observation of a cross-section at the top of the scaffold, C) magnified SEM view on the dense/cortical region of the scaffold, D) SEM observation of the macroporous structure, E) PIXE chemical mapping of silicon and calcium.

3.2. Scaffolds dissolution products preserve cells viability

BG-PCL dissolution profile in the culture medium was measured by ICP-AES every two days for a total period of 14 days. BG-PCL scaffolds were first preconditioned in the culture medium for 3 days (data not shown), which lead to a rise of Si (from 0 µg/ml to 55 µg/ml) and Ca (from 50 µg/ml to 85 µg/ml) concentrations in the medium as BG dissolves, and to a decrease of P concentration (from 27 µg/ml to 14 µg/ml). After preconditioning, Si concentration remained stable (approximately 50 µg/ml) for each time (**Figure. 2A**) and Ca and P were consistently consumed after renewing the medium with a slight decrease in

concentrations (Ca: from 50 to 40 µg/ml and P: from 27 to 22 µg/ml), supporting apatite precipitation and bioactivity of BG-PCL.[16] In order to characterize the impact of these concentration modulations following BG-PCL incubation, the cell viability of RPO was assessed using a XTT-based assay (**Figure. 2B**). Preconditioned BG-PCL was compared to a commercial bovine xenograft (BTB) and to the native control medium (baseline ion concentration) and the materials were not in contact with cells (indirect culture). After 7 days of culture, the cell viability was similar in the three conditions. The absence of significant difference discloses the absence of adverse effects of BG-PCL dissolution products on cell growth and proliferation.

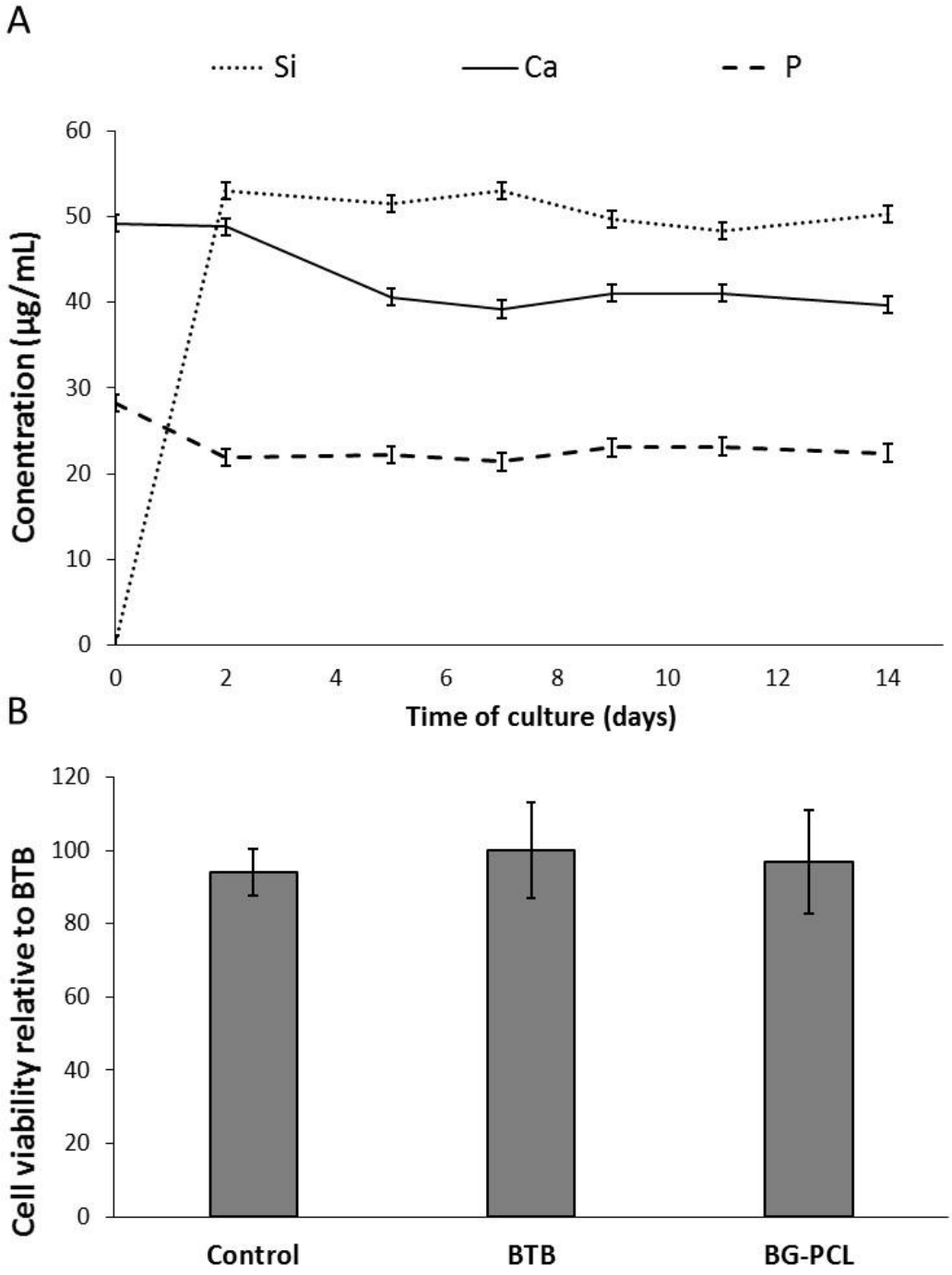

Figure 2. A) Evaluation of BG-PCL dissolution products by ICP-AES. Concentrations in Si, Ca and P were measured in the collected media after their interaction with preconditioned BG-PCL and compared to the original culture medium (t=0). B) RPO viability after 7 days of culture in the presence of preconditioned PCL-BG or BTB dissolution products compared with untreated cells (Ctrl).

3.3. BG-PCL hybrid scaffolds favor cell adhesion and spreading

The behavior of RPO on pure PCL disks, BG-PCL disks, and human cortical bone slices was investigated. SEM pictures show a poor adhesion of cells at the surface of pure PCL disks with a few small round cells that does not correspond to normal osteoblast phenotype (**Figure. 3A)**. In contrast, cells seeded on human cortical bone (**Figure. 3B**) and BG-PCL disks (**Figure. 3C**) cover the whole surface of the materials and exhibit spindle shapes and connected filopodia, thus demonstrating appropriate cell adhesion. Cells appear to spread even more at the surface of BG-PCL compared to human cortical bone. Cell adhesion was further investigated on BG-PCL scaffolds: similar cell shapes are observed (**Figures. 3D, 3E and 3F**) with a homogeneous distribution as evidenced by fluorescent imaging **(Figure. 3F)**, showing the uniform repartition of nuclei at the surface of the scaffold walls.

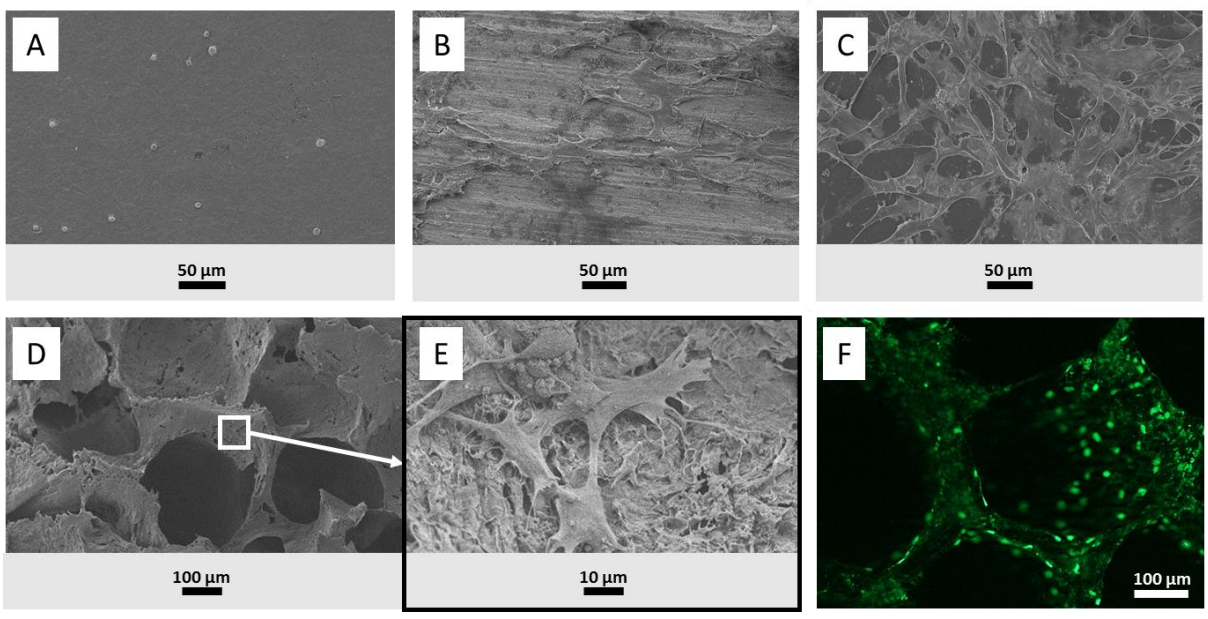

Figure 3. Representative SEM images of RPO cultured on A) PCL disks, B) human cortical bone, C) BG-PCL disks and D-E) inside BG-PCL scaffolds. F) Distribution of RPO inside BG-PCL scaffolds as observed by fluorescence microscopy.

To further investigate cell adhesion mechanisms on BG-PCL, we examined the phosphorylation of the focal adhesion kinase protein on its tyrosine 397 (pFAK) which is characteristic of the cellular adhesion process. pFAK proteins were detected from RPO cultivated 12 hours in BTB and BG-PCL scaffolds (n=6) **(Figure. 4A)** supporting the establishment of focal contacts with both materials. pFAK/FAK ratio was used to quantify cell adhesion **(Figure. 4B)**. As illustrated, the pFAK/FAK ratio is higher when cells are cultured in BG-PCL scaffolds, supporting a greater cell adhesion with the hybrid compared to BTB consistently with the SEM observations. Protein extraction from scaffold biomaterials remains challenging. To ensure that even protein amounts were properly loaded into gels an additional GAPDH blotting was performed and showed no significant variation. Interestingly, in this light, the FAK/GAPDH ratio reveals that the total form of the FAK protein is significantly higher in cellular extracts from BG-PCL compared to BTB **(Figure. 4C)**.

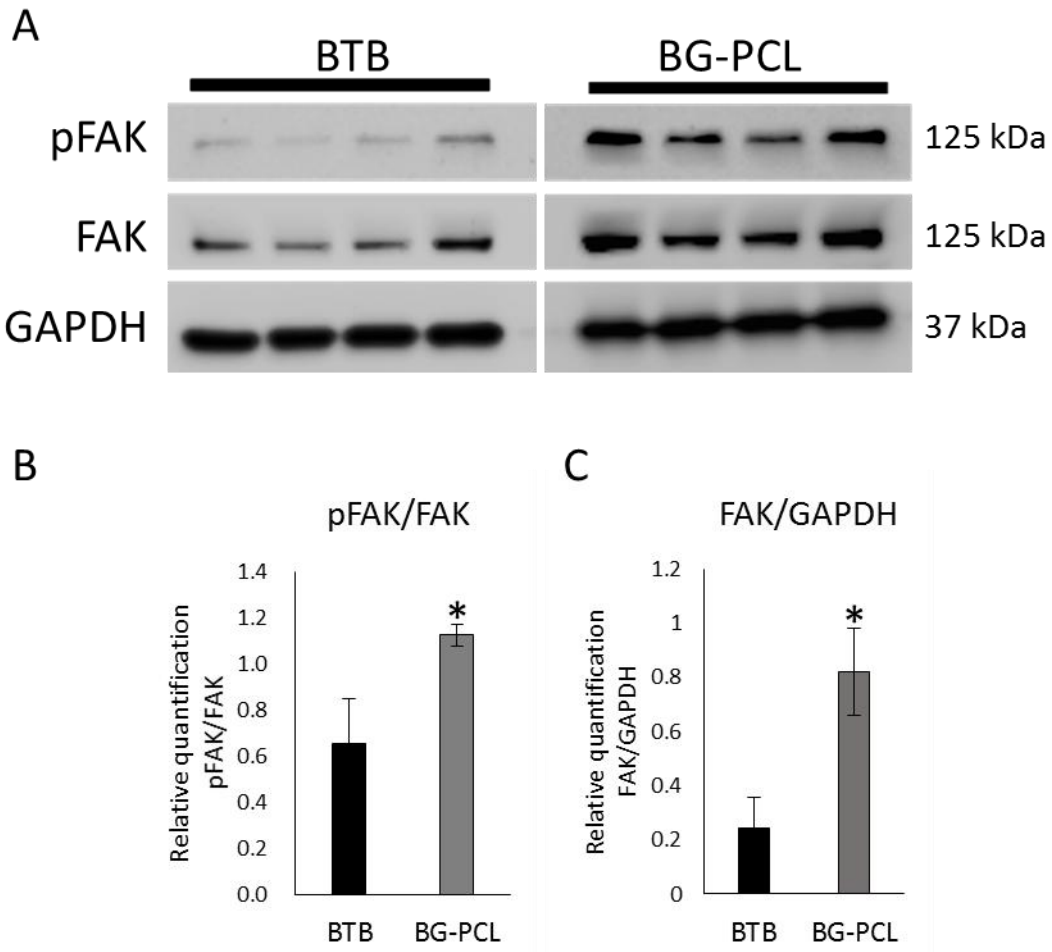

Figure 4. Pro-adhesive potential of BG-PCL scaffolds in comparison with BTB after 12h culture of rat primary osteoblast (RPO). A) Western blot analysis of FAK and pFAK expressions in RPO cells. B) Relative quantification of pFAK/FAK and C) FAK relative to GAPDH. (±SD; *$p<0.05$).

3.4. Osteogenic potential of BG-PCL scaffolds

The osteogenic potential of BG-PCL scaffolds was assessed by measuring the expression of Runx2 protein and the activity of alkaline phosphatase (ALP) two markers of the osteoblastic lineage differentiation. As observed by western blot (**Figure. 5A),** RPO cultured 7 or 14 days in BG-PCL scaffolds and BTB without osteogenic factor supplementation both express Runx2

protein. However, the quantification reveals that Runx2 expression was greater when cells were grown inside BG-PCL scaffolds (+60% at D7, +40% at D7). Likewise, the ALP activity was significantly higher (21 fold) in BG-PCL after 14 days of culture **(Figure. 5B)**.

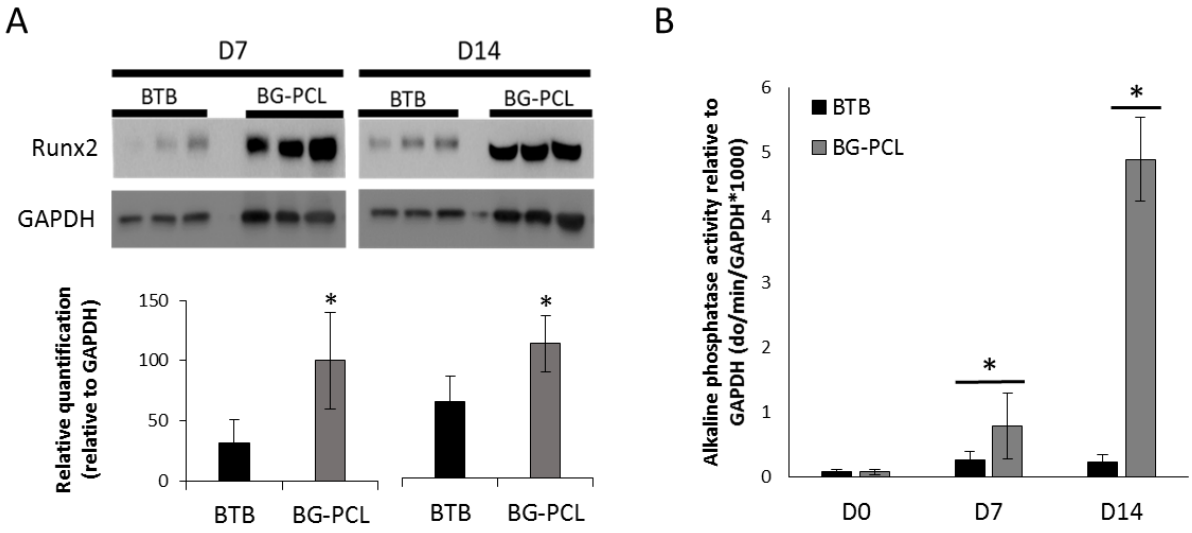

Figure 5. Osteogenic potential of BG-PCL compared to BTB. Runx2 expression A) and enzymatic ALP activity B) of RPO after 7 and 14 days of culture in BG-PCL scaffolds or BTB. (±SD; *p<0.05).

3.5. BG-PCL scaffolds evaluation in a mice model of critical-size calvarial defects

Healing of critical-size mouse calvarial defects was evaluated using micro-CT. The post-operative scan highlights the X-ray radiolucency of BG-PCL scaffolds (**Figure. 6A, BG-PCL D0**) that allows an easy monitoring of bone regeneration for BG-PCL scaffolds. After 30 days of implantation, empty defects show a slight bone regeneration of about 10% (**Figure. 6B**) emerging from the edges (**Figure. 6A, Empty D30**). Defects filled with BTB show an equivalent regeneration rate with limited peripheral bone reconstruction. In contrast, a significantly higher bone volume (approximately 20%) is measured in defects filled with BG-

PCL scaffolds at day 30 (**Fig. 6B**). Remarkably, with BG-PCL scaffolds bone repair is no longer limited to the edges (**Fig. 6A, BG-PCL D90**) but extends to the whole defect. At the end of the experiment, bone volume in Sham controls and BTB-filled defects has reached less than 15%, while more than 30% of the defect is repaired when employing BG-PCL scaffolds (**Fig. 6B**).

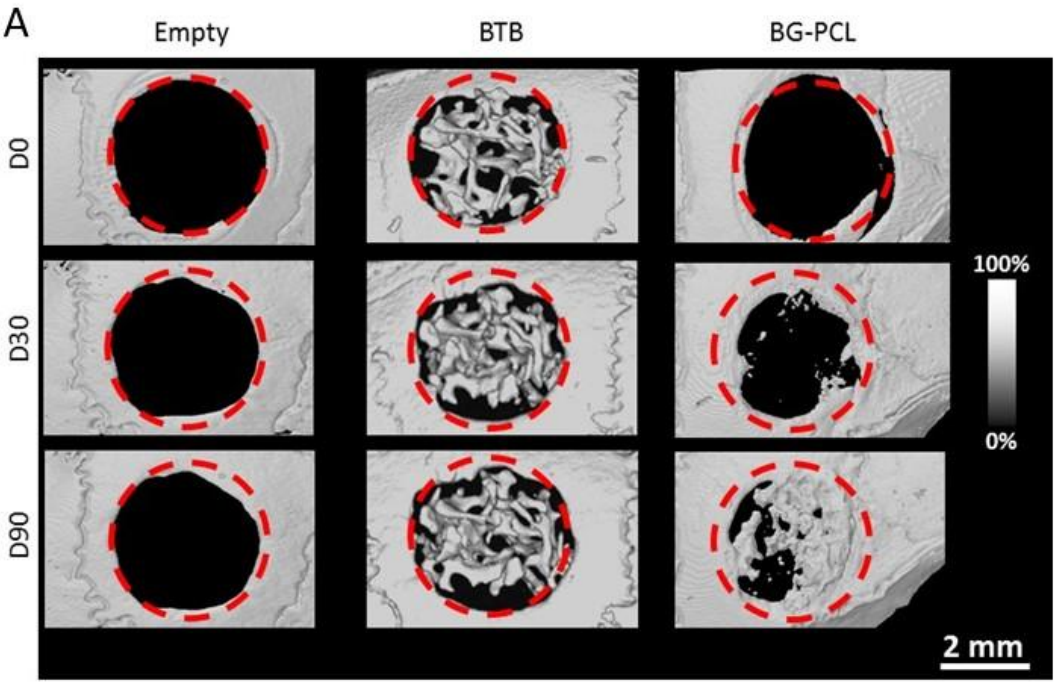

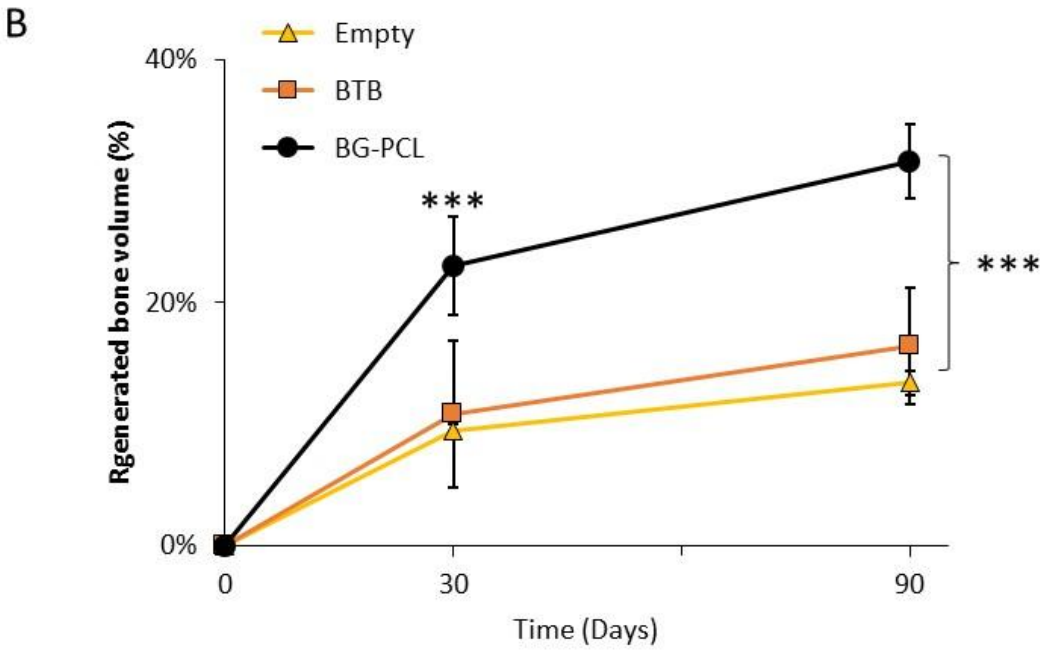

Figure 6. Bone ingrowth in a critical-size mice calvaria defect. A) Micro-CT images of bone defects left empty ("Sham" control) or filled with BTB or BG-PCL scaffolds. Images were obtained right after implantation (D0), after 30 days (D30) or 90 days implantation (D90). B) Quantitative analysis of bone regeneration in defects expressed in percentage of reconstruction (± SD, *p<0.05, ***p: 0.001).

3.6. BG-PCL is replaced by minerals and support bone remodeling

After 90 days of implantation, calvaria were collected for histological analyses. Mineral deposition was assessed by Alizarin red and Von Kossa staining (**Figure. 7**). The presence of mineralized tissue is observed in both BG-PCL and BTB samples. A histomorphometric comparison between the two materials was not possible due to the composition of BTB that makes it difficult to distinguish BTB from newly formed bone. However, only a few mineralized areas which correspond to the bovine bone's trabeculae are observed in the BTB-filled defects while defects implanted with BG-PCL scaffolds present a homogeneous mineralization.

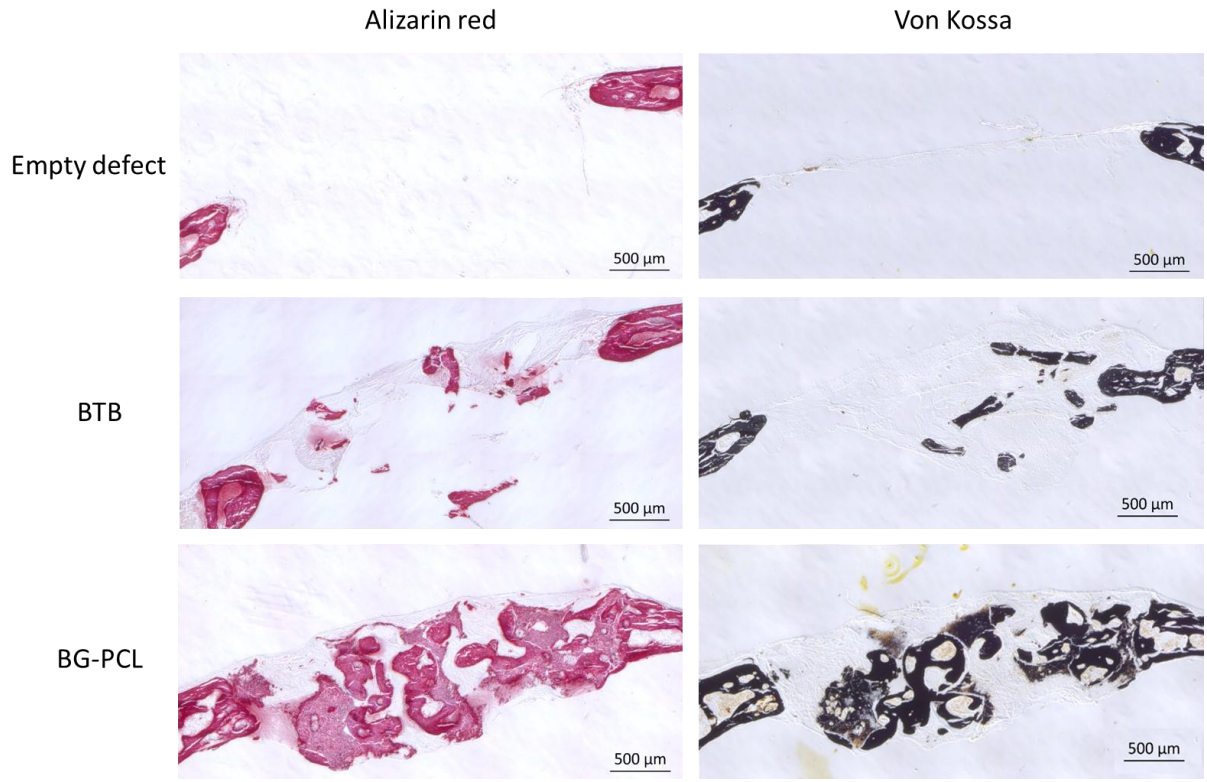

Figure 7. Histological appearance of critical defects in mice calvaria 90 days after surgery. Frontal demineralized tissue sections were subjected to Alizarin red or Von Kossa stainings to visualize respectively calcium in pink or calcium phosphate in black.

A modified Masson-Goldner trichrome staining highlights the identification of collagen fibers in green and the subsequent bone formation. There is no bone ingrowth when the defect is left empty (**Figure. 8A**). In contrast, the presence of new mature bone (dark green) is observed in defects filled with BG-PCL (**Figure. 8C**) whereas a collagen network of lower density (light green) is observed when defects were filled with BTB (**Figure. 8B**). Besides, the magnification (**Figure. 8E-F**) attests the presence of osteoblasts, osteoid tissues and resorption pits demonstrating that the newly formed bone is being remodeled in BG-PCL samples. The cellular management of this bone remodeling is further evidenced by a positive staining of TRAP (**Figure. 8D**) and ALP (**Figure. 8FG)** in BG-PCL samples (BTB ALP and TRAP stainings are available in the supplemental data). Additionally, samples were tested for specific bone formation markers.

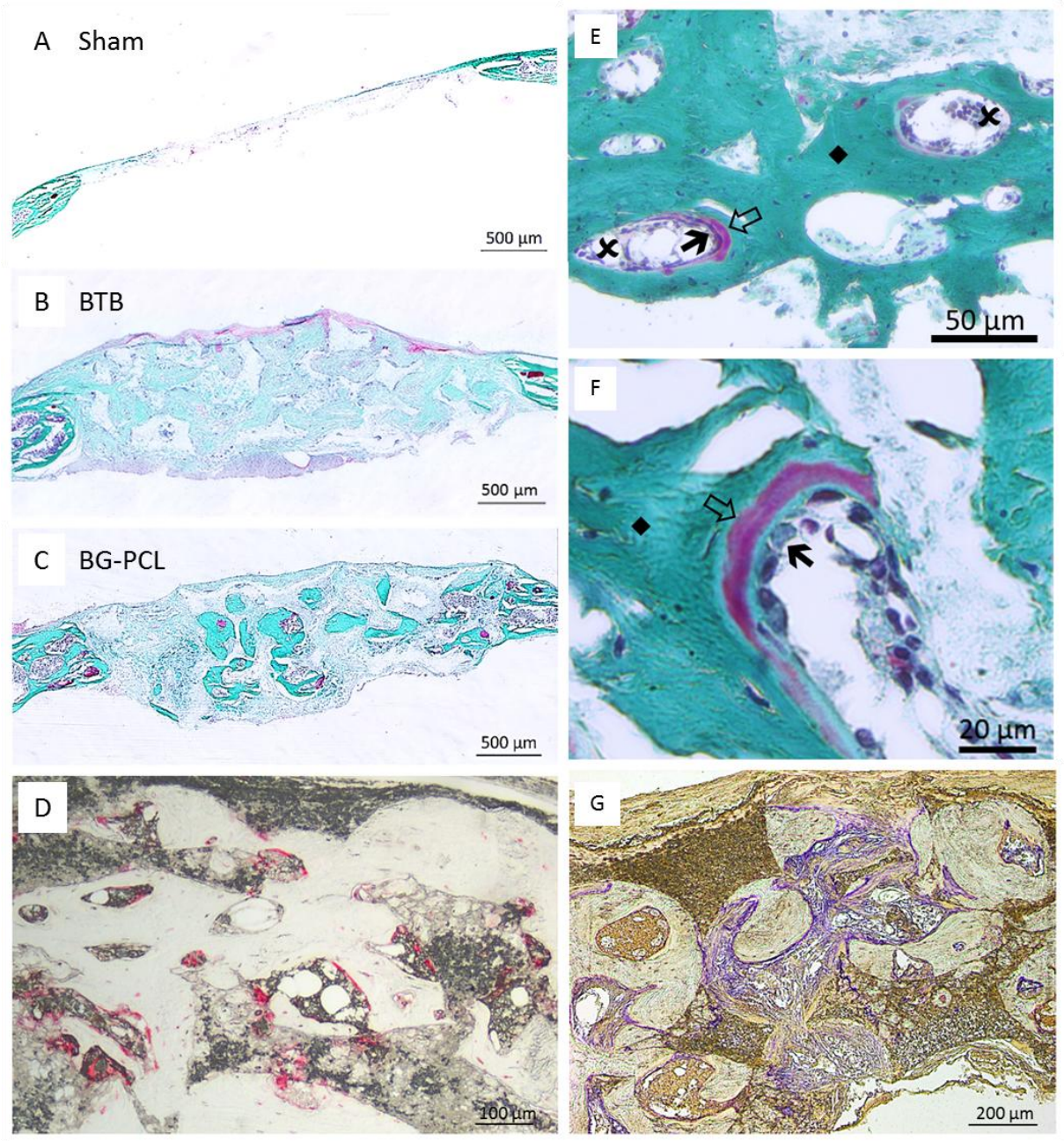

Figure 8. Histological appearance of calvarial critical defects left empty A) or filled with BTB B) or BG-PCL scaffolds C-G) after 90 days of implantation. Frontal demineralized tissue sections were subjected to modified Masson-Goldner trichrome (A-B, E-F) to visualize collagen (green), osteoid tissues (pink/red) and bone cell nuclei (dark purple). (◆: Mineralized bone tissue; ⇗: osteoid; ➚: osteoblasts; ✕: resorption lacuna). Bone remodeling activity was also highlighted for BG-PCL by enzymatic staining of TRAP (red) F) or ALP (purple) G).

According to **Figures 9A-C**, the expression of osteopontin can be detected in BG-PCL filled defects while no osteopontin expression is observed for the BTB and defects left empty. Interestingly, a positive staining of endomucin is also observed in BG-PCL samples and reveals the presence of blood vessels (**Figure. 9D**). Taken together, these data strongly support a great osteogenic potential of the hybrid, potential that is widely superior to the bovine xenograft to achieve a full bone regeneration process.

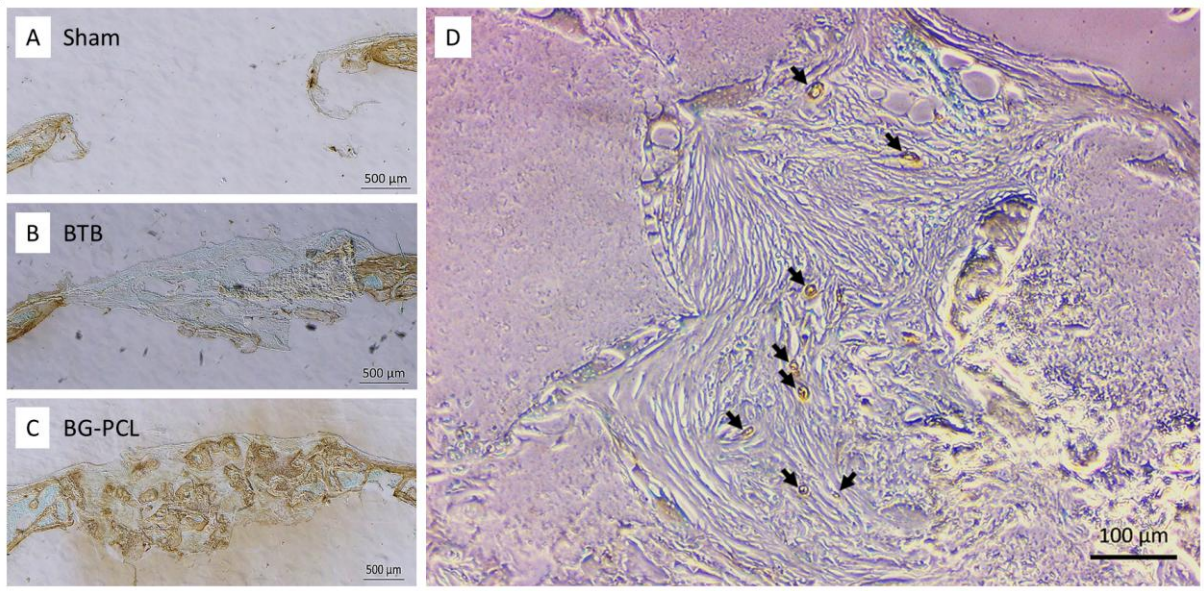

Figure 9. A–C Osteopontin identification by immunohistochemistry. A) Empty defect, B) BTB, C) BG-PCL, and D) endomucine identification for BG-PCL after 90 days of implantation in calvarial critical defects (arrows point positive endomucine staining).

Unstained histological sections were subjected to chemical changes analysis of BG-PCL scaffolds during implantation in mice calvarial defects. **Figures 10A–C** show the remaining BG-PCL scaffolds embedded in a newly-formed bone matrix. Although difficult to distinguish it from bone tissues, remaining BG-PCL can be identified with respect to their higher optical density as visible from **figure 10A**, and have been encircled in green in **figure 10B**. The initial composition of the BG-PCL scaffolds was 30 wt% BG/ 70 wt% PCL, with

the chemical composition of the BG being SiO_2 (75 wt%) – CaO (25 wt%). This corresponds to the following overall inorganic elemental composition for the BG-PCL hybrid: 10.5 wt% Si – 5.4 wt% Ca (and it is worth mentioning: 0% P). Remarkably, **figure 10B-C** show the complete chemical transformation of the remaining BG-PCL. After 90 days implantation in the mouse calvaria, BG-PCL scaffolds have been massively changed into a calcium phosphate, with a uniform distribution of Ca and P elements throughout the scaffold walls, making it hardly distinguishable from the surrounding new bone tissues (**Figure. 10C**). Elemental concentrations have been measured in the different areas of the histological sections: the remaining BG-PCL areas and newly-formed bone areas, and results are displayed in **figure 10D**. The remaining BG-PCL and newly-formed bone tissues exhibit very similar inorganic composition after 90 days, even with respect to trace elements content like sulphur (S) and magnesium (Mg). The incorporation of calcium and phosphorus into the BG-PCL has been massive: the BG-PCL is now composed of 38 wt% Ca and 17.5 wt% P, to be compared with the initial starting composition (10.5 wt% Si – 5.4 wt% Ca – 0 wt% P), which did not contain any phosphorus. As a result of the mineralization of the BG-PCL scaffolds, only very low amount of Si remains in the material (1281 +/- 303 ppm average value). Since measured Si concentration in the surrounding newly-formed bone tissue is at similar trace levels (1600 +/- 652 ppm average value), we can infer that Si has been successfully excreted out of the implantation site.

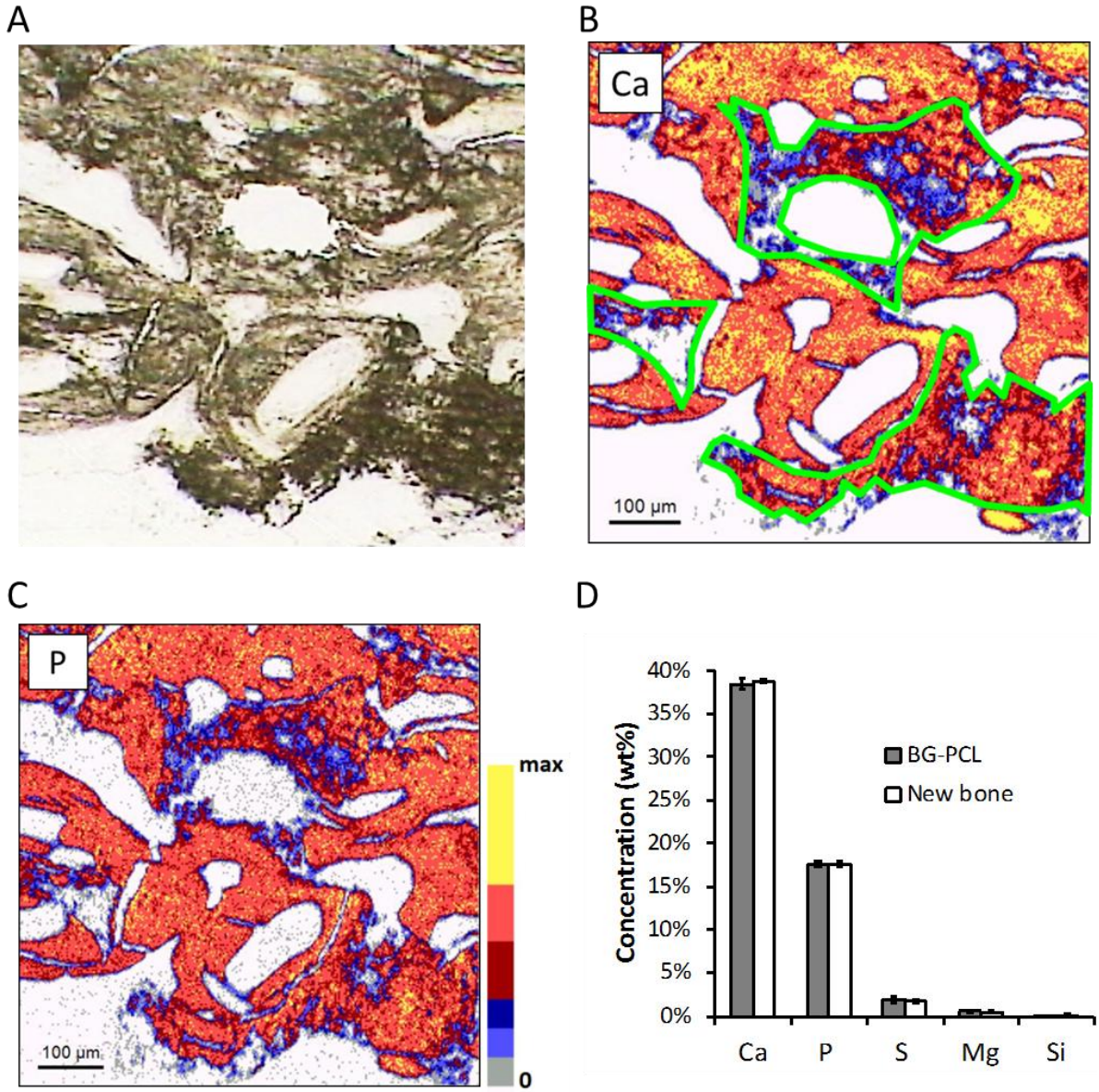

Figure 10. A-C) Histological section of BG-scaffold and regenerated bone after 90 days implantation in critical-size mice calvarial defects, A) optical view, B) PIXE chemical mapping of calcium and C) PIXE chemical mapping of phosphorus. D) Measures of the elemental concentrations in areas corresponding to remaining BG-PCL or newly-formed bone.

4. Discussion

In order to test the clinical relevance of our biomaterial, BG-PCL hybrids were compared to Lubboc^{TM}, a commercial bone substitute used in orthopedic or periodontal surgery procedures. Lubboc^{TM} is a purified xenogenic graft made from bovine trabecular bone. Due to a physical and chemical purification process (T650), Lubboc^{TM} is a non-antigenic and non-pyrogenic material scaffold with porosity and mechanical properties quite similar to human bone that qualified it as an adequate candidate for challenging control conditions.[27] To date, a study from the University Hospital of Patras (Greece) had compared *in vivo* the efficacy of Lubboc^{TM} to autograft, demineralized allograft (Grafton^{TM}) and biphasic calcium phosphate (Ceraform^{TM}) a commercialized synthetic biomaterial.[28] The bovine xenogenic grafts was ranked as the second best in term of bone formation and quality of the newly-formed bone, just below autografts and significantly better than the others two making it a challenging benchmark for the evaluation of BG-PCL hybrids.

BG-PCL properties were first evaluated *in vitro* using primary osteoblast cells from rat calvaria (RPO). RPO is a well acknowledged model to study osteoblast physiology and behavior in the context of bone formation,[29,30] along with the osteogenic properties and cytotoxicity of biomaterials.[31–34] SEM imaging and fluorescent microscopy combined with cell viability assays highlighted the capacity of rat osteoblasts to adhere and proliferate at the surface of BG-PCL hybrids. Accordingly, western blot analyses evidenced a stimulation of the FAK pathway when cells were grown on BG-PCL. FAK is a cytoplasmic protein kinase localized in focal adhesions and involved in cells adhesion. Autophosphorylation of FAK on its Y397 residue induced by clustered integrins marks its activation and leads to the formation of a complex with paxillin at nascent adhesion.[35] The evaluation of the Y397 level of FAK is therefore an effective method to study the strength of cell adhesion. Interestingly, this western blot study (**Fig. 4A**) did not only show a higher level of the phosphorylated Y397 FAK in

BG-PCL in comparison with Lubboc^{TM} but also a greater expression of the total protein. As FAK participates to cell survival (PI3-K/Akt), cell spreading and migration (ERK/MAPK),[36] this modulation of the total protein level by BG-PCL may also contribute to promote osteoblast proliferation and commitment. These mechanisms remain to be investigated.

Using dynamic conditions, we further highlighted the biological potential of BG-PCL hybrid scaffolds as demonstrated by a progressive increase of ALP activity greater than BTB in non-osteogenic medium. This osteogenic potential was confirmed by a greater expression of the transcription factor Runx2 when cells were grown in BG-PCL (compared to BTB). The enhanced stimulation of RPO by BG-PCL may be related to dissolution products. Si is released from BG-PCL leading to a rapid increase of Si concentration reaching ≈ 50 µg/mL and remaining stable thereafter. This Si plateau corresponds to the limit of the orthosilicic acid ($Si(OH)_4$) solubility in an aqueous medium which is 58 µg/mL.[37] This Si concentration range is known to stimulate osteoblasts differentiation and proliferation[38,39] and is thought to be partly responsible for the observed osteogenic properties of bioactive glasses [38].

Critical-size defects in mouse calvaria allow the implantation of biomaterials in orthotopic sites in a highly standardized way without the need of external fixations.[40] However, the regeneration of such defects is challenging due to the poor vascularization of the site and the absence of periosteum which is removed during the surgery. To date, the percentage of regenerated bone (corresponding to the ratio of newly-formed bone volume over the defect volume) for pure BG scaffolds implanted in critical-size calvarial defects in similar models after 12 weeks range from 8.5 to 19%. For instance : (1) 8.5 %–14.9 % for 13-93 bioactive glass scaffolds with 50% porosity and 50–500 µm pore size,[41] (2) 12.4 % for 45S5 particles,[41] (3) 19 % for 13-93 scaffolds with trabecular structures close to that of present BG-PCL scaffolds, owing 80% porosity and 100–500 µm pore sizes.[42] In our hands, BG-PCL hybrid

scaffolds lead to 31.6 % (+/- 3%) regenerated bone which is about twice more than what was observed for the bovine xenograft gold standard.

Histological analyses highlighted the presence of dense mineralized collagen deposited by osteoblasts and resorption pits created by osteoclasts. This physiological bone remodeling process is further supported by alkaline phosphatase (ALP) and tartrate resistant acid phosphatase (TRAP) activities.[43] In addition, endomucin, a sialoglycoprotein secreted by endothelial cells of early blood capillaries was detected inside BG-PCL scaffolds after 3 months of implantation supporting vessel sprouting which is essential for the physiological regeneration of bone.[44,45] Taken together, these data highlight that the bone healing process driven by the BG-PCL hybrid involves a full cell-mediated process associated with a mineralization driven by the intrinsic chemical reactivity of the BG and the hybrid's ability to promote a vascular network to deliver cell precursors, oxygen and nutrients.

Besides BG-PCL biological properties, the dual cortical/trabecular feature opens a new avenue of particular interest for guided bone regeneration applications in cranio-facial surgery such as dehiscence-and fenestration-type defects around dental implant[46] or maxillary sinus augmentation where a membrane is positioned on the buccal mucosa to prevent colonization by fibrous tissue.[47]

5. Conclusion

In the present study, we have investigated the biological potential of a hybrid scaffold made of BG (SiO_2-CaO) and PCL owing a dual cortical/trabecular structure. *In vitro* and *in vivo* experiments demonstrate the ability of BG-PCL to favor cell adhesion, to stimulate osteoblast differentiation and activity without adding any osteogenic supplementary differentiation factors and to support vascularization and bone ingrowth at higher levels than the bovine xenograft (Lubboc^{TM}) known for its performance. Furthermore, (1) the X-ray translucency allows an easy *in situ* evaluation of bone regeneration; (2) the dual cortical/trabecular

morphology opens attractive perspectives in guided bone regeneration; and (3) the synthesis route at room temperature represents an potent opportunity for the direct incorporation of temperature-sensitive substances like osteogenic factors or drugs for further enhancement of BG-PCL biological properties that may represent a breakthrough innovation in the field.

Conflict of interest: NONE

Acknowledgments:

The authors thank the Fonds Européen De Développement Régional (FEDER) and the Auvergne Rhône-Alpes regional council for funding. Dr Mhammed Benbakkar and the Laboratoire Magma et Volcans (UMR 6524, CNRS/Université Clermont Auvergne) are acknowledged for ICP-AES measurements. The Centre d'Études Nucléaires de Bordeaux-Gradignan and the AIFIRA staff are acknowledged for allowing the PIXE experiments. Dr. Brigitte Gaillard- Martinie, the Plateau Technique de Microscopie du Centre INRA ARA (UMR 454, MEDIS) and the Centre Imagerie Cellulaire Santé (Faculté de Médecine de Clermont-Ferrand) are acknowledged for SEM imaging of cells on biomaterials. Pr. Catherine Chaussain and the Laboratoires Pathologies, Imagerie et Biothérapies orofaciales (EA 2496) are acknowledged for the animal study.

OST-Développement company (Clermont-Ferrand, France) is acknowledged for providing the Lubboc^{TM} and cortical bone samples and for carrying out the sterilization of the materials.

Bibliography

(1) Hench, L. L.; Paschall, H. A. Direct Chemical Bond of Bioactive Glass-Ceramic Materials to Bone and Muscle. *J. Biomed. Mater. Res.* **1973**, *7* (3), 25–42. https://doi.org/10.1002/jbm.820070304.

(2) Cao, W.; Hench, L. L. Bioactive Materials. *Ceram. Int.* **1996**, *22* (6), 493–507. https://doi.org/10.1016/0272-8842(95)00126-3.

(3) Hoppe, A.; Güldal, N. S.; Boccaccini, A. R. A Review of the Biological Response to Ionic Dissolution Products from Bioactive Glasses and Glass-Ceramics. *Biomaterials* **2011**, *32* (11), 2757–2774. https://doi.org/10.1016/j.biomaterials.2011.01.004.

(4) Leu, A.; Leach, J. K. Proangiogenic Potential of a Collagen/Bioactive Glass Substrate. *Pharm. Res.* **2008**, *25* (5), 1222–1229. https://doi.org/10.1007/s11095-007-9508-9.

(5) Munukka, E.; Leppäranta, O.; Korkeamäki, M.; Vaahtio, M.; Peltola, T.; Zhang, D.; Hupa, L.; Ylänen, H.; Salonen, J. I.; Viljanen, M. K.; et al. Bactericidal Effects of Bioactive Glasses on Clinically Important Aerobic Bacteria. *J. Mater. Sci. Mater. Med.* **2008**, *19* (1), 27–32. https://doi.org/10.1007/s10856-007-3143-1.

(6) Stoor, P.; Söderling, E.; Salonen, J. I. Antibacterial Effects of a Bioactive Glass Paste on Oral Microorganisms. *Acta Odontol. Scand.* **1998**, *56* (3), 161–165.

(7) Fu, Q.; Saiz, E.; Rahaman, M. N.; Tomsia, A. P. Bioactive Glass Scaffolds for Bone Tissue Engineering: State of the Art and Future Perspectives. *Mater. Sci. Eng. C* **2011**, *31* (7), 1245–1256. https://doi.org/10.1016/j.msec.2011.04.022.

(8) Niemela, T.; Niiranen, H.; Kellomaki, M.; Tormala, P. Self-Reinforced Composites of Bioabsorbable Polymer and Bioactive Glass with Different Bioactive Glass Contents. Part I: Initial Mechanical Properties and Bioactivity. *Acta Biomater.* **2005**, *1* (2), 235–242. https://doi.org/10.1016/j.actbio.2004.11.002.

(9) Jones, J. R. Review of Bioactive Glass: From Hench to Hybrids. *Acta Biomater.* **2013**, *9* (1), 4457–4486. https://doi.org/10.1016/j.actbio.2012.08.023.

(10) Yu, B.; Turdean-Ionescu, C. A.; Martin, R. A.; Newport, R. J.; Hanna, J. V.; Smith, M. E.; Jones, J. R. Effect of Calcium Source on Structure and Properties of Sol-Gel Derived Bioactive Glasses. *Langmuir ACS J. Surf. Colloids* **2012**, *28* (50), 17465–17476. https://doi.org/10.1021/la303768b.

(11) Maeno, S.; Niki, Y.; Matsumoto, H.; Morioka, H.; Yatabe, T.; Funayama, A.; Toyama, Y.; Taguchi, T.; Tanaka, J. The Effect of Calcium Ion Concentration on Osteoblast Viability, Proliferation and Differentiation in Monolayer and 3D Culture. *Biomaterials* **2005**, *26* (23), 4847–4855. https://doi.org/10.1016/j.biomaterials.2005.01.006.

(12) Li, A.; Shen, H.; Ren, H.; Wang, C.; Wu, D.; Martin, R. A.; Qiu, D. Bioactive Organic/Inorganic Hybrids with Improved Mechanical Performance. *J. Mater. Chem. B* **2015**, *3* (7), 1379–1390. https://doi.org/10.1039/C4TB01776E.

(13) Poologasundarampillai, G.; Yu, B.; Tsigkou, O.; Wang, D.; Romer, F.; Bhakhri, V.; Giuliani, F.; Stevens, M. M.; McPhail, D. S.; Smith, M. E.; et al. Poly(γ-Glutamic Acid)/Silica Hybrids with Calcium Incorporated in the Silica Network by Use of a Calcium Alkoxide Precursor. *Chem. Weinh. Bergstr. Ger.* **2014**, *20* (26), 8149–8160. https://doi.org/10.1002/chem.201304013.

(14) Poologasundarampillai, G.; Yu, B.; Jones, J. R.; Kasuga, T. Electrospun Silica/PLLA Hybrid Materials for Skeletal Regeneration. *Soft Matter* **2011**, *7* (21), 10241. https://doi.org/10.1039/c1sm06171b.

(15) Lao, J.; Dieudonné, X.; Fayon, F.; Montouillout, V.; Jallot, E. Bioactive Glass–Gelatin Hybrids: Building Scaffolds with Enhanced Calcium Incorporation and Controlled Porosity for Bone Regeneration. *J Mater Chem B* **2016**, *4* (14), 2486–2497. https://doi.org/10.1039/C5TB02345A.

(16) Bossard, C.; Granel, H.; Jallot, E.; Vial, C.; Tiainen, H.; Wittrant, Y.; Lao, J. Polycaprolactone / Bioactive Glass Hybrid Scaffolds for Bone Regeneration. *Biomed. Glas.* **2018**, *4*, 108–122. https://doi.org/doi.org/10.1515/bglass-2018-0010.

(17) Gunawidjaja, P. N.; Izquierdo-Barba, I.; Mathew, R.; Jansson, K.; García, A.; Grins, J.; Arcos, D.; Vallet-Regí, M.; Edén, M. Quantifying Apatite Formation and Cation Leaching from Mesoporous Bioactive Glasses in Vitro: A SEM, Solid-State NMR and Powder XRD Study. *J. Mater. Chem.* **2012**, *22* (15), 7214. https://doi.org/10.1039/c2jm15066b.
(18) Antoun, H.; Karouni, M.; Sojod, B. La Régénération Osseuse Guidée : Résultats, Limites et Perspectives. *Actual. Odonto-Stomatol.* **2013**, No. 261, 11–21. https://doi.org/10.1051/aos/2013103.
(19) Ma, Z.; Gao, C.; Gong, Y.; Shen, J. Paraffin Spheres as Porogen to Fabricate Poly(L-Lactic Acid) Scaffolds with Improved Cytocompatibility for Cartilage Tissue Engineering. *J. Biomed. Mater. Res. B Appl. Biomater.* **2003**, *67* (1), 610–617. https://doi.org/10.1002/jbm.b.10049.
(20) Bellows, C. G.; Aubin, J. E.; Heersche, J. N. M.; Antosz, M. E. Mineralized Bone Nodules Formedin Vitro from Enzymatically Released Rat Calvaria Cell Populations. *Calcif. Tissue Int.* **1986**, *38* (3), 143–154. https://doi.org/10.1007/BF02556874.
(21) Bellows, C. G.; Aubin, J. E.; Heersche, J. N. M. Initiation and Progression of Mineralization of Bone Nodules Formed in Vitro: The Role of Alkaline Phosphatase and Organic Phosphate. *Bone Miner.* **1991**, *14* (1), 27–40. https://doi.org/10.1016/0169-6009(91)90100-E.
(22) Ishida, H. Characterization of the 1,25-(OH)2D3-Induced Inhibition of Bone Nodule Formation in Long-Term Cultures of Fetal Rat Calvaria Cells. *Endocrinology* **1993**, *132* (1), 61–66. https://doi.org/10.1210/en.132.1.61.
(23) Radin, S.; Ducheyne, P.; Rothman, B.; Conti, A. The Effect of in Vitro Modeling Conditions on the Surface Reactions of Bioactive Glass. *J. Biomed. Mater. Res.* **1997**, *37* (3), 363–375.
(24) Wu, S.-C. Influence of Hydrodynamic Shear Stress on Microcarrier-Attached Cell Growth: Cell Line Dependency and Surfactant Protection. *Bioprocess Eng.* **1999**, *21* (3), 201. https://doi.org/10.1007/s004490050663.
(25) Perez, R. A.; Riccardi, K.; Altankov, G.; Ginebra, M.-P. Dynamic Cell Culture on Calcium Phosphate Microcarriers for Bone Tissue Engineering Applications. *J. Tissue Eng.* **2014**, *5*, 2041731414543965. https://doi.org/10.1177/2041731414543965.
(26) Collignon, A.-M.; Lesieur, J.; Anizan, N.; Azzouna, R. B.; Poliard, A.; Gorin, C.; Letourneur, D.; Chaussain, C.; Rouzet, F.; Rochefort, G. Y. Early Angiogenesis Detected by PET Imaging with 64Cu-NODAGA-RGD Is Predictive of Bone Critical Defect Repair. *Acta Biomater.* **2018**, *82*, 111–121. https://doi.org/10.1016/j.actbio.2018.10.008.
(27) Poumarat, G.; Squire, P. Comparison of Mechanical Properties of Human, Bovine Bone and a New Processed Bone Xenograft. *Biomaterials* **1993**, *14* (5), 337–340.
(28) Athanasiou, V. T.; Papachristou, D. J.; Panagopoulos, A.; Saridis, A.; Scopa, C. D.; Megas, P. Histological Comparison of Autograft, Allograft-DBM, Xenograft, and Synthetic Grafts in a Trabecular Bone Defect: An Experimental Study in Rabbits. *Med. Sci. Monit. Int. Med. J. Exp. Clin. Res.* **2010**, *16* (1), BR24-31.
(29) Aronow, M. A.; Gerstenfeld, L. C.; Owen, T. A.; Tassinari, M. S.; Stein, G. S.; Lian, J. B. Factors That Promote Progressive Development of the Osteoblast Phenotype in Cultured Fetal Rat Calvaria Cells. *J. Cell. Physiol.* **1990**, *143* (2), 213–221. https://doi.org/10.1002/jcp.1041430203.
(30) Abe, Y.; Aida, Y.; Abe, T.; Hirofuji, T.; Anan, H.; Maeda, K. Development of Mineralized Nodules in Fetal Rat Mandibular Osteogenic Precursor Cells: Requirement for Dexamethasone but Not for Beta-Glycerophosphate. *Calcif. Tissue Int.* **2000**, *66* (1), 66–69.
(31) Liao, H. Response of Rat Osteoblast-like Cells to Microstructured Model Surfaces in Vitro. *Biomaterials* **2003**, *24* (4), 649–654. https://doi.org/10.1016/S0142-9612(02)00379-4.
(32) Wirth, C.; Grosgogeat, B.; Lagneau, C.; Jaffrezic-Renault, N.; Ponsonnet, L. Biomaterial Surface Properties Modulate in Vitro Rat Calvaria Osteoblasts Response: Roughness and or Chemistry? *Mater. Sci. Eng. C* **2008**, *28* (5–6), 990–1001. https://doi.org/10.1016/j.msec.2007.10.085.
(33) Hayes, J. S.; Khan, I. M.; Archer, C. W.; Richards, R. G. The Role of Surface Microtopography in the Modulation of Osteoblast Differentiation. *Eur. Cell. Mater.* **2010**, *20*, 98–108.
(34) Washington, J. T.; Schneiderman, E.; Spears, R.; Fernandez, C. R.; He, J.; Opperman, L. A. Biocompatibility and Osteogenic Potential of New Generation Endodontic Materials

Established by Using Primary Osteoblasts. *J. Endod.* **2011**, *37* (8), 1166–1170. https://doi.org/10.1016/j.joen.2011.05.011.
(35) Choi, C. K.; Zareno, J.; Digman, M. A.; Gratton, E.; Horwitz, A. R. Cross-Correlated Fluctuation Analysis Reveals Phosphorylation-Regulated Paxillin-FAK Complexes in Nascent Adhesions. *Biophys. J.* **2011**, *100* (3), 583–592. https://doi.org/10.1016/j.bpj.2010.12.3719.
(36) Westhoff, M. A.; Serrels, B.; Fincham, V. J.; Frame, M. C.; Carragher, N. O. Src-Mediated Phosphorylation of Focal Adhesion Kinase Couples Actin and Adhesion Dynamics to Survival Signaling. *Mol. Cell. Biol.* **2004**, *24* (18), 8113–8133. https://doi.org/10.1128/MCB.24.18.8113-8133.2004.
(37) Belton, D. J.; Deschaume, O.; Perry, C. C. An Overview of the Fundamentals of the Chemistry of Silica with Relevance to Biosilicification and Technological Advances. *FEBS J.* **2012**, *279* (10), 1710–1720. https://doi.org/10.1111/j.1742-4658.2012.08531.x.
(38) Xynos, I. D.; Edgar, A. J.; Buttery, L. D.; Hench, L. L.; Polak, J. M. Ionic Products of Bioactive Glass Dissolution Increase Proliferation of Human Osteoblasts and Induce Insulin-like Growth Factor II MRNA Expression and Protein Synthesis. *Biochem. Biophys. Res. Commun.* **2000**, *276* (2), 461–465. https://doi.org/10.1006/bbrc.2000.3503.
(39) Xynos, I. D.; Edgar, A. J.; Buttery, L. D.; Hench, L. L.; Polak, J. M. Gene-Expression Profiling of Human Osteoblasts Following Treatment with the Ionic Products of Bioglass 45S5 Dissolution. *J. Biomed. Mater. Res.* **2001**, *55* (2), 151–157.
(40) Gomes, P. S.; Fernandes, M. H. Rodent Models in Bone-Related Research: The Relevance of Calvarial Defects in the Assessment of Bone Regeneration Strategies. *Lab. Anim.* **2011**, *45* (1), 14–24. https://doi.org/10.1258/la.2010.010085.
(41) Bi, L.; Jung, S.; Day, D.; Neidig, K.; Dusevich, V.; Eick, D.; Bonewald, L. Evaluation of Bone Regeneration, Angiogenesis, and Hydroxyapatite Conversion in Critical-Sized Rat Calvarial Defects Implanted with Bioactive Glass Scaffolds. *J. Biomed. Mater. Res. A* **2012**, *100* (12), 3267–3275. https://doi.org/10.1002/jbm.a.34272.
(42) Liu, X.; Rahaman, M. N.; Fu, Q. Bone Regeneration in Strong Porous Bioactive Glass (13-93) Scaffolds with an Oriented Microstructure Implanted in Rat Calvarial Defects. *Acta Biomater.* **2013**, *9* (1), 4889–4898. https://doi.org/10.1016/j.actbio.2012.08.029.
(43) Katsimbri, P. The Biology of Normal Bone Remodelling. *Eur. J. Cancer Care (Engl.)* **2017**, *26* (6). https://doi.org/10.1111/ecc.12740.
(44) Mercado-Pagán, Á. E.; Stahl, A. M.; Shanjani, Y.; Yang, Y. Vascularization in Bone Tissue Engineering Constructs. *Ann. Biomed. Eng.* **2015**, *43* (3), 718–729. https://doi.org/10.1007/s10439-015-1253-3.
(45) Liu, C.; Shao, Z. M.; Zhang, L.; Beatty, P.; Sartippour, M.; Lane, T.; Livingston, E.; Nguyen, M. Human Endomucin Is an Endothelial Marker. *Biochem. Biophys. Res. Commun.* **2001**, *288* (1), 129–136. https://doi.org/10.1006/bbrc.2001.5737.
(46) Elgali, I.; Omar, O.; Dahlin, C.; Thomsen, P. Guided Bone Regeneration: Materials and Biological Mechanisms Revisited. *Eur. J. Oral Sci.* **2017**, *125* (5), 315–337. https://doi.org/10.1111/eos.12364.
(47) Li, X.; Chen, S.; Zhu, S.; Zha, G. Guided Bone Regeneration Using Collagen Membranes for Sinus Augmentation. *Br. J. Oral Maxillofac. Surg.* **2012**, *50* (1), 69–73. https://doi.org/10.1016/j.bjoms.2010.10.013.

ToC:

Organic-inorganic hybrid scaffolds with dual cortical/trabecular porosity have been designed using bioactive glass and polycaprolactone. These highly porous scaffolds associate ductile mechanical properties and bioactivity. They support osteoblasts adhesion and differentiation

in vitro (rat primary osteoblasts) and promote bone regeneration *in vivo* (mouse critical calvaria defects) more efficiently than a commercial xenograft control.

ToC keyword:

Hybrid scaffolds.

ToC figure: